

See discussions, stats, and author profiles for this publication at: <https://www.researchgate.net/publication/263291948>

# Atomic Structure and Dynamics of Metal Dopant Pairs in Graphene

ARTICLE *in* NANO LETTERS · JUNE 2014

Impact Factor: 13.59 · DOI: 10.1021/nl500682j · Source: PubMed

---

CITATIONS

13

---

READS

59

## 9 AUTHORS, INCLUDING:



[Kuang He](#)

University of Oxford

37 PUBLICATIONS 447 CITATIONS

[SEE PROFILE](#)



[Alex W Robertson](#)

University of Oxford

44 PUBLICATIONS 785 CITATIONS

[SEE PROFILE](#)



[Angus I Kirkland](#)

University of Oxford

260 PUBLICATIONS 3,806 CITATIONS

[SEE PROFILE](#)



[Gun-Do Lee](#)

Seoul National University

65 PUBLICATIONS 867 CITATIONS

[SEE PROFILE](#)

# Atomic Structure and Dynamics of Metal Dopant Pairs in Graphene

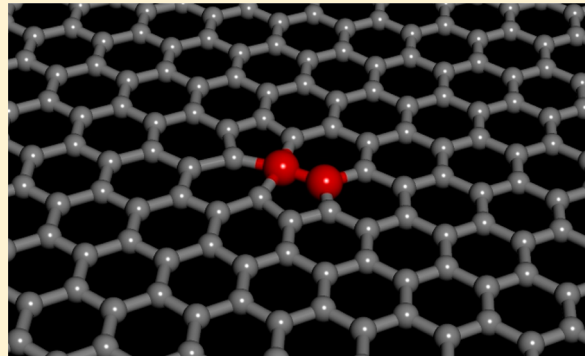
Zhengyu He,<sup>†</sup> Kuang He,<sup>†</sup> Alex W. Robertson,<sup>†</sup> Angus I. Kirkland,<sup>†</sup> Dongwook Kim,<sup>§</sup> Jisoohn Ihm,<sup>§</sup> Euijoon Yoon,<sup>‡</sup> Gun-Do Lee,<sup>‡,\*</sup> and Jamie H. Warner<sup>\*,†</sup>

<sup>†</sup>Department of Materials, University of Oxford, Parks Road, Oxford, OX1 3PH, United Kingdom

<sup>‡</sup>Department of Material Science and Engineering and <sup>§</sup>Department of Physics and Astronomy, Seoul National University, Seoul 151-742, Korea

## S Supporting Information

**ABSTRACT:** We present an atomic resolution structural study of covalently bonded dopant pairs in the lattice of monolayer graphene. Two iron (Fe) metal atoms that are covalently bonded within the graphene lattice are observed and their interaction with each other is investigated. The two metal atom dopants can form small paired clusters of varied geometry within graphene vacancy defects. The two Fe atoms are created within a 10 nm diameter predefined location in graphene by manipulating a focused electron beam (80 kV) on the surface of graphene containing an intentionally deposited Fe precursor reservoir. Aberration-corrected transmission electron microscopy at 80 kV has been used to investigate the atomic structure and real time dynamics of Fe dimers embedded in graphene vacancies. Four different stable structures have been observed; two variants of an Fe dimer in a graphene trivacancy, an Fe dimer embedded in two adjacent monovacancies and an Fe dimer trapped by a quadvacancy. According to spin-sensitive DFT calculations, these dimer structures all possess magnetic moments of either 2.00 or 4.00  $\mu_B$ . The dimer structures were found to evolve from an initial single Fe atom dopant trapped in a graphene vacancy.



**KEYWORDS:** Graphene, dopants, HRTEM, metal, AC-TEM

Controlling the key properties of graphene<sup>1</sup> including band structure,<sup>2,3</sup> carrier concentration,<sup>4–6</sup> and particularly magnetism<sup>7</sup> broadens its utilization as a new functional material for nanoelectronic applications. One promising approach for modifying the properties of graphene is to introduce impurity dopants, such as metal atoms, substitutionally, interstitially, or as surface adatoms. Calculations on single transition metal (TM) atoms and clusters adsorbed on graphene reveal that as adsorbents they can induce local magnetic moments.<sup>8,9</sup> TM adsorbents can move freely on the surface of pristine graphene and this limits the use of surface adatoms as robust and reliable dopants for nanoelectronic and magnetic applications that require precise, stable structural configurations. To overcome this difficulty, forming stable TM-doped graphene samples by substitutional or interstitial doping is promising.<sup>10,11</sup>

Available techniques for introducing dopants into graphene include the synthesis of hybridized graphene,<sup>12,13</sup> intercalation,<sup>14,15</sup> chemical modification,<sup>16,17</sup> low energy ion implantation,<sup>18</sup> and defect-assisted doping by electron beam irradiation.<sup>19</sup> Among these methods, the defect-assisted doping method has demonstrated nanoscale spatial control of dopant placement. In this method, a vacancy is first created in graphene within a typically  $10 \times 10 \text{ nm}^2$  area by focused electron beam irradiation using an aberration-corrected transmission electron microscope (AC-TEM) operated at an accelerating voltage of

80 kV.<sup>20</sup> These vacancies show enhanced chemical reactivity and are able to trap mobile TM atoms, which are theoretically predicted to exhibit local magnetic moments.<sup>21</sup> Using a suitably sculpted electron beam to create the defect sites that trap metal atoms to form stable dopants also enables the *in situ* study of the structure of the impurity atoms and their migration dynamics.

AC-TEM has enabled the study of single metal atom dopants as well as multatom small clusters of metal atoms interacting with graphene surfaces and edges. Cretu et al.<sup>22</sup> have observed a large spatial oscillation of a W atom on a graphene sheet between two reconstructive defects and a smaller vibration localized at one trapping center using high-resolution transmission electron microscope (HR-TEM) that revealed the mechanism of strain-induced adsorption. Robertson et al.<sup>19</sup> reported real time dynamics of single Fe atoms embedded in graphene vacancies and their possible migration paths. In this work, impurities were shown to induce pronounced displacements of the adjacent carbon atoms when hopping into the vacancy sites.<sup>19</sup> Furthermore, examination of a single Fe atom in a divacancy defect using aberration-corrected scanning

**Received:** February 22, 2014

**Revised:** May 21, 2014

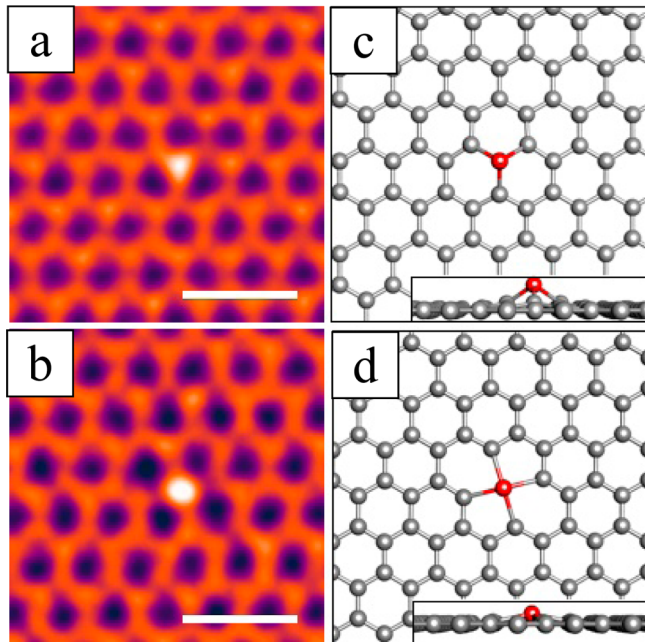
**Published:** June 19, 2014



transmission electron microscope (AC-STEM) and electron energy loss spectroscopy showed a resistance to oxidation of the Fe atom.<sup>23</sup> AC-STEM and AC-TEM have also been employed to investigate the interactions of single and of multiatom Si<sub>6</sub> clusters at the edges of graphene.<sup>24,25</sup> However, the study of paired metal atoms interacting with graphene is limited, especially as covalently bonded pairs within the graphene lattice.

Here, we report the atomic structure of stable configurations of Fe atom pairs incorporated into the 2D planar structure of graphene. The monolayer graphene was synthesized by CVD growth on a Cu catalyst using previously reported conditions.<sup>26</sup> Using residual surface contamination on the top surface of graphene as the source of Fe or Si atoms limits further development in the area and it is better to deposit controlled predefined amounts of a dopant. In this study, we have intentionally added Fe dopant atoms to the surface of graphene by drop casting solutions of FeCl<sub>3</sub> onto clean graphene samples. This results in a larger number of mobile Fe atoms on the surface of the graphene and facile filling of vacancies with Fe atoms, compared to relying purely on surface residues as the source of dopant atoms. Subsequently, vacancy sites in a defined region are created through irradiation with a focused electron beam.<sup>20</sup> We have observed four stable structures formed from graphene vacancies embedded with an Fe dimer and their mutual transformations. We have also calculated the magnetic moments of these configurations using DFT, in addition to the binding energy of the second Fe atom. This combination of theory and experiment has enabled us to propose possible mechanisms for the transformations observed.

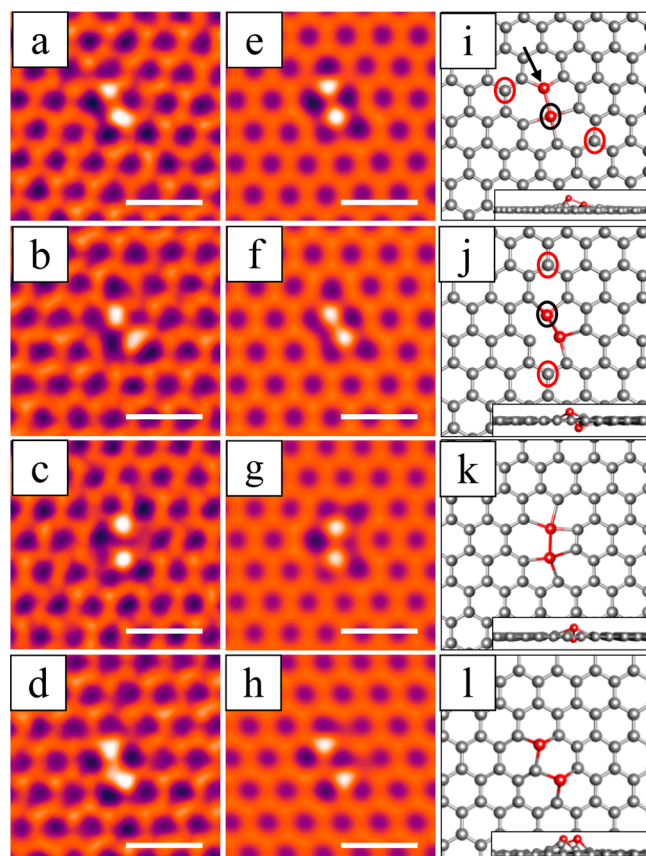
As with previous observations, monovacancies and divacancies in graphene act as trap sites for mobile individual Fe atoms leading to the formation of two well-known Fe dopant configurations,<sup>19</sup> shown in Figure 1. Figure 1a is an AC-TEM



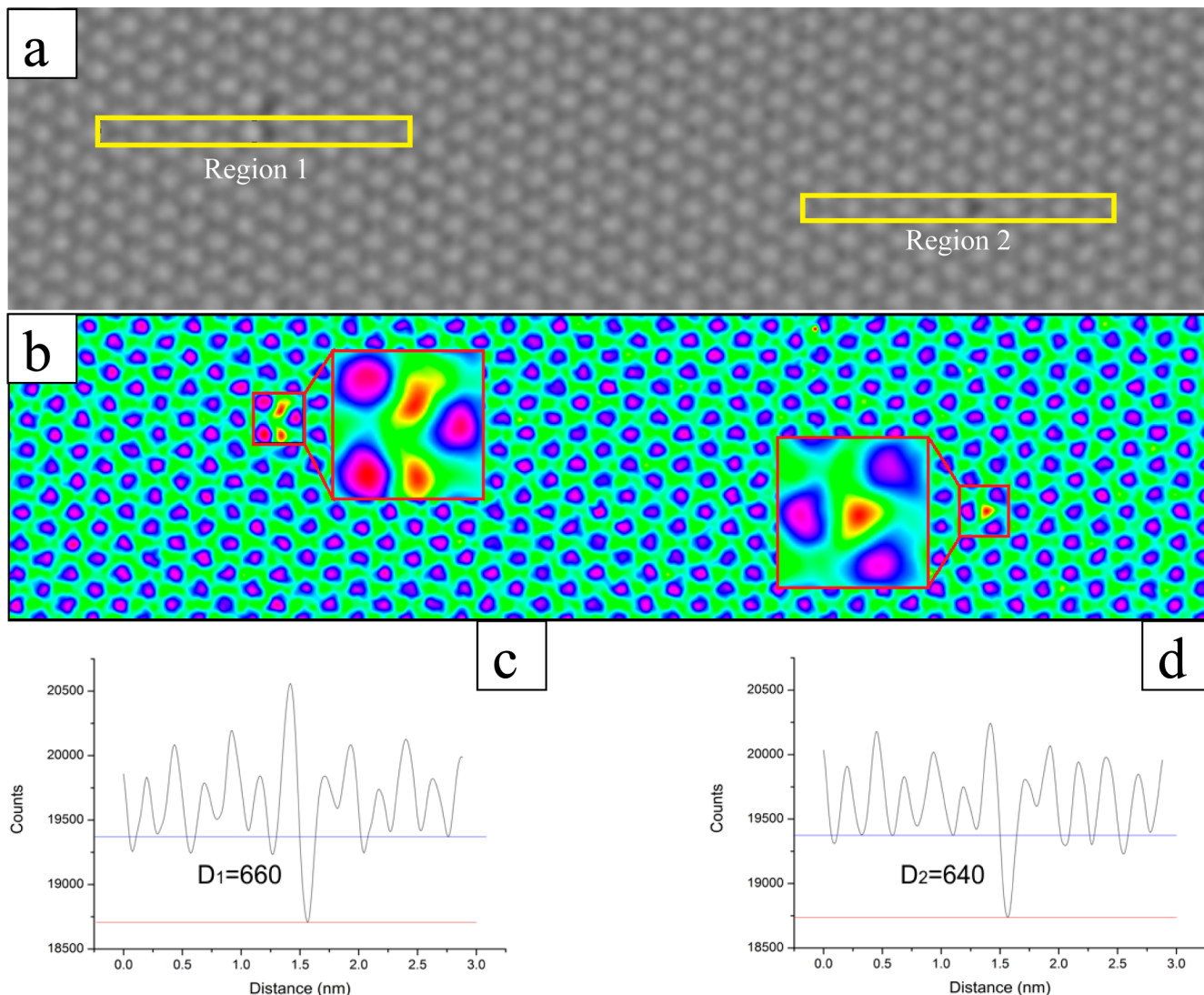
**Figure 1.** Single Fe atoms in graphene vacancies. (a,b) Smoothed AC-TEM images of single Fe atoms in (a) monovacancy and (b) divacancy sites shown in false color. (c,d) DFT optimized atomic models corresponding to (a,b). Inset to (c,d) show the side views of the optimized structures. Scale bar: 0.5 nm.

image of an Fe atom in a monovacancy (i.e., 1 Fe atom replaces 1 C atom) and Figure 1b is an Fe atom in a divacancy (i.e., 1 Fe atom replaces 2 C atoms). Front views of density functional theory (DFT) calculated atomic models are presented in Figure 1c,d and insets show the side views of these two different single Fe atom dopant structures. It is often the case that another Fe atom is trapped within the graphene lattice at a region further away and we subsequently consider these cases as two separate single atom dopants. However, if a second Fe atom is trapped at a lattice site adjacent to the initial Fe atom, we regard this as an Fe dimer. We observe that the trapping of two Fe atoms to form an Fe dimer happens sequentially with the initial formation of a single dopant site that then acts as trapping center for the second Fe atom. The energy driving this process comes primarily from the electron beam. We first created a vacancy using the focused electron beam. The vacancy has an attractive potential for the attachment of a mobile surface Fe atom and leads to the single Fe atom within the graphene lattice. When this single atom dopant is continuously irradiated by the electron beam it will also be reactive and act as an attractive potential for the trapping of a second Fe atom to form the Fe dimer

Figure 2a–d show four different Fe dimer (DiFe) structures observed in AC-TEM images together with multislice image



**Figure 2.** Fe dimers in graphene vacancies. Smoothed AC-TEM images of a pair of Fe atoms in (a) trivacancy (DiFe@TV\_1); (b) alternative trivacancy (DiFe@TV\_2); (c) quadvacancy (DiFe@QV) and (d) two adjacent monovacancies (DiFe@2MVs). (e–h) Multislice image simulations based on the DFT optimized atomic models shown in (i–l) respectively. Inset in panels (i–l) show side views of the optimized structures. Fe atoms are marked in red balls in (i–l). Scale bar: 0.5 nm in all images.



**Figure 3.** (a) Smoothed AC-TEM image of a region containing both an Fe dimer and a single Fe atom. (b) Smoothed AC-TEM image in (a) but displayed using a “spectrum” CLUT. Insets in (b) show the enlarged view of impurities areas. (c,d) Intensity profiles from region 1 and 2 (regions highlighted by a yellow box in (a)). Blue lines are the average charge-coupled device (CCD) counts values of the minimum values of carbon atoms and red lines are the CCD counts values of the minimum value of Fe atoms. The intensity differences between Fe atom and C atoms are 660 CCD counts and 640 CCD counts in (c,d), respectively.

simulations,<sup>27,28</sup> Figure 2e–h, based on the DFT calculated atomic models in Figure 2i–l. Figure 2a shows a pair of Fe atoms within a graphene trivacancy (TV), subsequently denoted as DiFe@TV\_1. In this structure, the Fe atom marked by a black circle in Figure 2i substitutes for two carbon atoms interstitially and hence bonds to 4 nearest neighboring atoms. The second Fe atom labeled by black arrow in Figure 2i replaces a carbon atom substitutionally, forming three covalent bonds with adjacent atoms. An alternative Fe dimer–graphene trivacancy complex structure is shown in Figure 2b, subsequently denoted DiFe@TV\_2. A difference between the DFT models of these two trivacancy complexes is that in DiFe@TV\_1 both Fe atoms sit slightly above the plane of the graphene sheet, while in the DiFe@TV\_2 case one of the Fe atoms is above and the other below the plane of the graphene sheet. This leads to an unequal distance between the Fe atom marked by a black circle and the two carbon atoms highlighted by red circles in Figure 2j with a difference of 82 pm while in the DiFe@TV\_1 structure; the equivalent difference is ca. 17

pm (see also Supporting Information Figure S1). According to DFT calculations, when two Fe atoms are trapped by a graphene trivacancy, the DiFe@TV\_2 structure is 1.03 eV energetically favored. However, our observations show that the DiFe@TV\_1 structure appears more frequently, which can be explained by the formation process of the two structures. The doping method we have utilized involved the deposition of an Fe precursor on only one side of the graphene sheet. Therefore, it is reasonable to believe that most mobile Fe atoms are located on one side of graphene, which may increase the probability for the formation of DiFe@TV\_1, where both of the atoms are at the same side of graphene. Contrary to that, forming DiFe@TV\_2 requires another Fe atom to diffuse through a vacancy to the other side of graphene. This may help to explain why the DiFe@TV\_1 appears more frequently in our TEM observations even though the total energy is higher than that of DiFe@TV\_2.

We have also observed an Fe dimer embedded in a graphene tetravacancy (we refer to the tetravacancy hereafter as

quadvacancy (QV) in order to avoid confusion with the acronym for the trivacancy (TV)) (Figure 2c), subsequently denoted DiFe@QV. In this structure two Fe atoms substitute two adjacent pairs of carbon atoms interstitially with both forming tetravalent nearest neighbor bonding configurations. Figure 2d shows an Fe dimer trapped by two adjacent graphene monovacancies in the same lattice site. In this configuration, each Fe atom substitutes for one carbon atom and forms three covalent bonds with its nearest neighbor and as such, is the only structure where two Fe atoms do not bond to each other directly.

In order to ensure we are observing Fe dimer complexes instead of the switching of single Fe atom dopants from one configuration to another within the acquisition time of the image (possibly giving the false appearance of two Fe atoms), we have measured the intensity box profiles within two yellow boxed regions from one image, shown in Figure 3a, across high intensity sites corresponding to impurity atoms. The region on the right shows a single Fe atom in a graphene monovacancy and provides a reference value for measurements from the Fe dimers on the left side. The image in Figure 3b uses a “spectrum” color look-up table (CLUT) and shows that the intensity at all three sites corresponding to heavy atoms is equivalent (insets to Figure 3b). Figure 3c,d shows intensity profiles corresponding to regions 1 and 2 (highlighted in yellow boxes in Figure 3a). The difference in intensity between dopant atoms in regions 1 and 2 compared to the carbon atoms in the graphene lattice indicates that the two dark spots in region 1 correspond to two Fe atoms and not a single atom hopping between graphene lattice sites.

Given our observation of stable Fe dimer structures, we have calculated the magnetic moments for each of the structures, reported in Table 1. To understand the role that the Fe dimer

**Table 1. Magnetic Moment of Different Complexes**

Structure	Fe@MV	Fe@DV	DiFe@TV_1	DiFe@TV_2	DiFe@QV	DiFe@2MVs
Magnetic Moment	0.00 $\mu_B$	3.55 $\mu_B$	2.00 $\mu_B$	4.00 $\mu_B$	4.00 $\mu_B$	2.00 $\mu_B$

plays in the magnetic properties of doped graphene, we have also included the magnetic moments of the corresponding vacancy structures. The magnetic moment of Fe@MV is 0, while a graphene monovacancy structure has a magnetic moment of  $\sim 1.5 \mu_B$ .<sup>29</sup> A graphene divacancy is nonmagnetic, while a single Fe atom within a graphene divacancy has a magnetic moment of  $3.55 \mu_B$ . These values are consistent with previously reported DFT calculations.<sup>29–31</sup> The magnetic moment of a graphene trivacancy increases from  $1.05 \mu_B$ <sup>32</sup> to  $2.00 \mu_B$  after two Fe atom are incorporated into this graphene vacancy to form the DiFe@TV\_1 or to  $4.00 \mu_B$  the DiFe@TV\_2 structure. A graphene quadvacancy possesses a magnetic moment of  $2.00 \mu_B$ ,<sup>32</sup> which rises to  $4.00 \mu_B$  after two Fe atoms are incorporated into this graphene vacancy. The DiFe@2MVs system is composed of two adjacent Fe@MV complexes and therefore is expected to be nonmagnetic due to the zero magnetic moment of a single Fe@MV. However, surprisingly the magnetic moment increases from 0, as previously reported, to  $2 \mu_B$ .<sup>31</sup> Considering that the corresponding vacancy site is also nonmagnetic,<sup>31</sup> we conclude that a noncovalent interaction

between two Fe atoms leads to the magnetization. To investigate the interaction distance of two Fe atoms we have created models of DiFe@2MVs at different separation distances (see Supporting Information Figure S2 and Table S2). DFT calculations reveal that structures with longer separation distances are nonmagnetic, indicating the localized nature of the interaction between two Fe atoms. To deeply understand this interaction, further investigation of the charge distribution of this structure is needed.

Continuous monitoring of Fe-doped graphene reveals that all Fe dimer structures start from a single Fe atom embedded in a graphene divacancy. Figure 4 shows two sets of sequential

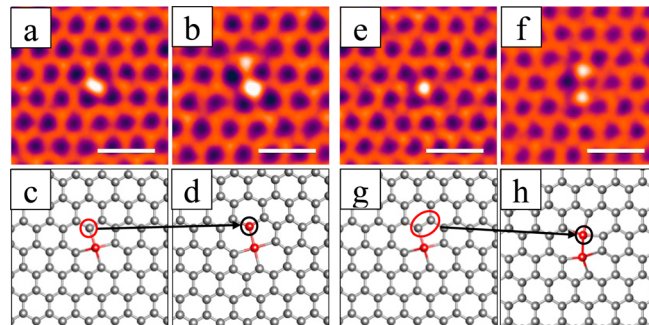


**Figure 4.** Transition from a single Fe dopant into an Fe dimer structure. (a–d) Transition from a single Fe atom- graphene divacancy complex (Fe@DV) into an Fe dimer trapped in a graphene trivacancy (DiFe@TV\_1). (a,b) Smoothed AC-TEM images of a single Fe atom trapped in a graphene divacancy (Fe@DV) and a pair of Fe impurities in a graphene trivacancy (DiFe@TV\_1). (c,d) DFT calculated atomic models corresponding to (a,b). Time difference between (a) and (b): 11 s. (e,h) Transition from Fe@DV to DiFe@QV. (e,f) Smoothed AC-TEM images of a single Fe atom trapped in a graphene divacancy (Fe@DV) and an Fe dimer in a graphene quadvacancy (DiFe@QV). (g,h) DFT calculated atomic models corresponding to (e,f). Time difference between (e) and (f): 19 s. Fe atoms are marked in red balls in (c,d,f,g). Scale bar for all images: 0.5 nm.

images and in both instances a second Fe atom joins an Fe@DV. Figure 4a,b shows a transition from the Fe@DV structure into DiFe@TV\_1 after 11s observation. Initially (Figure 4a), the Fe atom is located in a divacancy, bonded to 4 neighbors, and 11 s later a second Fe atom substitutes for the carbon atom marked by a red circle in the model shown in Figure 4c. This additional Fe atom (marked by a black circle in Figure 4d) is bonded to three C atoms effectively forming a pair of Fe impurities in a graphene trivacancy. In Figure 4e–h, another example of a transition from Fe@DV to DiFe@QV is illustrated. In this case, the starting state is also the Fe@DV structure and following a 19 s observation a pair of neighboring carbon atoms marked by a red ellipse in Figure 4g is removed from the graphene lattice and the vacancy created is occupied by an additional Fe atom (marked by a black circle in Figure 4h).

The transition described in Figure 4 is not just single-directional but is also reversible. Our observations show that an Fe dimer complex can return to an Fe@DV. Figure 5a–d shows the transition from DiFe@TV\_2 to Fe@DV. In this transition, the Fe atom (marked by a black circle in Figure 5c) is replaced by a carbon atom (marked by a red circle in Figure 5d). The original Fe atom changes coordination from two C atoms and one Fe atom in the DiFe@TV\_2 structure to four carbon atoms in the Fe@DV structure, as illustrated by the

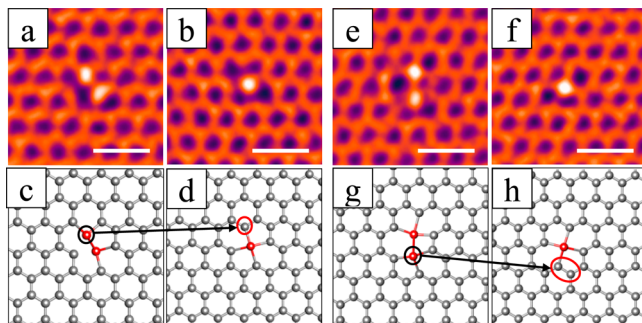


**Figure 5.** Transitions from the Fe dimer structure to single Fe complexes. (a–d) Transition from DiFe@TV\_2 to Fe@DV. (a,b) Smoothed AC-TEM images of DiFe@TV\_2 and Fe@DV, respectively. (c,d) Corresponding DFT calculated atomic models. Time difference between (a) and (b): 22 s. (e–h) Transition from DiFe@QV to Fe@DV. (e,f) Smoothed AC-TEM images of DiFe@QV and Fe@DV, respectively. (g,h) Corresponding DFT calculated atomic models. Time difference between (e,f): 23 s. Scale bar: 0.5 nm.

atomic models in Figure 5c,d. The DiFe@QV structure is also found to revert to a single Fe atom in divacancy structure as illustrated in Figure 5e–h. In this transition, the Fe atom marked by a black circle in Figure 5g is replaced by a carbon dimer. The mechanism of the loss of an Fe atom in the cases described here needs to be clarified. Robertson et al.<sup>19</sup> have proposed that a single Fe atom dopant in graphene vacancy is less likely to be sputtered away by the electron beam at acceleration voltage of 80 kV due to the high mass and binding energy of over  $-6$  eV<sup>21</sup> while the maximum energy transferred to the Fe atom is only  $E_m = 3.4$  eV.

To understand the mechanism behind, we have calculated the binding energy ( $E_b$ ) and the sputtering energy ( $E_s$ ) of DiFe@TV\_1, DiFe@TV\_2, and DiFe@QV, respectively, which are shown in Figure 6. The binding energy is the energy

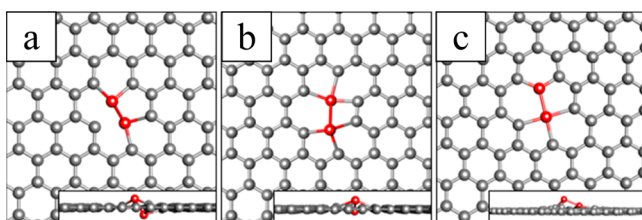


**Figure 6.** Sputtering and binding energy for Fe atom in (a) DiFe@TV\_2, (b) DiFe@QV, and (c) DiFe@TV\_1.

required to remove one of the Fe atoms from the Fe dimer and onto the surface of graphene. The sputtering energy is the energy required to remove one of the Fe atoms from the Fe dimer into the vacuum, which is higher than the binding energy. For all three cases in Figure 6, the sputtering energy is significantly higher than the maximum energy transferred by an 80 keV electron. Therefore, it is unlikely that the Fe atom within the dimer can be directly sputtered to vacuum. However, if we consider the binding energies in Figure 6, we see that DiFe@TV\_1 has a binding energy that is less than  $E_m$  and therefore it is possible that a single Fe atom can be ejected from the Fe dimer and onto the surface of graphene. Once on the surface of graphene, the energy barrier for migration along the

surface is small and at room temperature the Fe atom will move away from the region of interest, leaving a single Fe atom dopant.

In Figure 5, the initial Fe dimer structures that are observed to transform to the single Fe dopant are DiFe@TV\_2 and DiFe@QV, but Figure 6 shows the binding energy of these two Fe dimers is larger than  $E_m$  and therefore it is likely that an intermediate state between the initial and final states in Figure 5 occurs. We observed that many of the Fe dimers were able to switch back and forth between different configurations, as shown in Figure 7. It is possible that both the DiFe@TV\_2 and

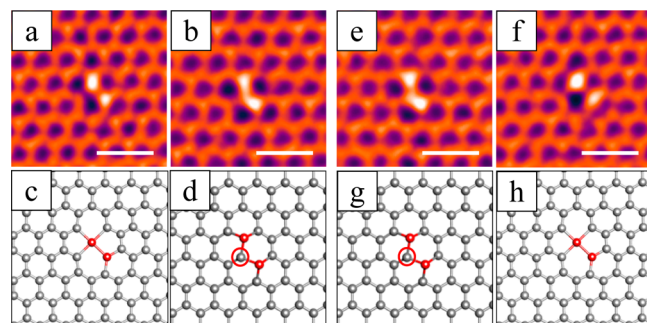


**Figure 7.** Swapping between two Fe dimer-graphene vacancies complexes. (a–d) Transition from DiFe@TV\_1 to DiFe@2MVs. (a,b) Smoothed AC-TEM images of DiFe@TV\_1 and DiFe@2MVs, respectively. (c,d) Corresponding DFT calculated atomic models. Time difference between (a) and (b): 7 s. (e–h) Transition from DiFe@2MVs to DiFe@TV\_1. (e,f) Smoothed AC-TEM images of DiFe@TV\_1 and DiFe@2MVs, respectively. (g,h) DFT calculated atomic models. Time difference between (e) and (f): 9 s. Scale bar: 0.5 nm.

DiFe@QV undergo transformation into the low binding energy structure, DiFe@TV\_1, through electron beam irradiation, and once in configuration of DiFe@TV\_1 it will be possible for an Fe atom to be ejected onto the surface by the energy transferred by the electron beam. However, due to the limitation of temporal resolution no intermediate state has been captured in our images. Because fewer occurrences of the Fe dimer DiFe@TV\_1 are observed in our results, it suggests that this structure can quickly transform to the single Fe atom dopant structure. The necessary addition of carbon atoms that mediates the transitions between different Fe dimers arises from residual carbon on the surface of the graphene and its mobilization by the electron beam.

The Fe dimer-vacancy structures are relatively stable under electron beam irradiation but show local changes in bonding configurations in particular switching between DiFe@TV\_1 and DiFe@2MVs. Figure 7a–d illustrates the transition from DiFe@TV\_1 to DiFe@2MVs with a carbon atom hopping (marked by red circle in Figure 7d) in between two Fe atoms. It is likely that the additional carbon atom is initially trapped by the defect and resides on top of the Fe dimer. Subsequently, it migrates to an in-plane site moving the two Fe atoms apart and weakening the covalent bond between the two Fe atoms that form three new bonds to neighboring carbon atoms. The reverse transition is illustrated in Figure 7e–h, which is initiated by the loss of one carbon atom (marked by red circle in Figure 7g) sputtered away by electron beam.

Fe dimer-vacancy complexes show better magnetic stability than single Fe dopants in graphene vacancies due to the magnetic moments of the four reported structures and their

mutual transformations. The incorporation of these complexes in devices that exploit their magnetic behavior requires a comprehensive understanding of the evolution process of the formation of dimer structure. In this regard, our observations that Fe dimer structures initiate from an Fe@DV suggests that a monovacancy or divacancy in graphene can only initially trap a single Fe atom rather than trapping two atoms simultaneously.

**Conclusion.** We have created spatially predefined vacancy sites in graphene with 10 nm spatial accuracy and used these to form Fe-dimer dopants in graphene. The introduction of an additional Fe source from concentrated  $\text{FeCl}_3$  enables the formation of Fe atoms pair-graphene vacancy complexes. Our observations reveal that all Fe dimer structures start from a single Fe atom in a graphene divacancy. Graphene vacancies with Fe dimer incorporated are relatively stable but were observed to undergo bonding configuration changes through a swapping between two dimer structures, or to change from an Fe dimer structure to single Fe atom residing in graphene divacancy. Spin-sensitive DFT calculations indicate that the magnetic moments of the various defect structures vary between  $2.00 \mu_B$  to  $4.00 \mu_B$ . We suggest that the dimer structure and its ability to transform could provide additional possibilities for the manipulation of carrier states with potential applications in graphene based spintronics.<sup>33</sup> This approach for dimer doping of graphene has the potential to be expanded to other elements such as Si.

**Methods. Synthesis of Graphene.** Graphene was synthesized using atmospheric pressure chemical vapor deposition of methane on a copper catalyst. The reaction conditions were as previously reported in ref 26. Briefly, a  $1 \text{ cm}^2$  piece of copper foil (Alfa Aesar, Puratronic 99.8% pure,  $25 \mu\text{m}$  thick) is loaded into a 1 in. quartz tube within a split-tube furnace CVD system. A gas flow of 100 sccm  $\text{H}_2/\text{Ar}$  (25% gas mix) and 200 sccm pure Ar was applied to the system while ramping from room temperature to  $1060^\circ\text{C}$  with the sample initially resting outside the hot zone of the furnace. Once the furnace reached  $1060^\circ\text{C}$ , the sample is moved into the hot zone and annealed for 1 h. Then the  $\text{CH}_4$  flow (1% gas mix in Ar) was activated at 10 sccm and the  $\text{H}_2/\text{Ar}$  flow reduced from 100 to 30 sccm, while maintaining the pure argon gas line flow at 200 sccm. These conditions were maintained for another 1 h to obtain continuous graphene film growth. Following this the  $\text{CH}_4$  flow was disabled and the sample immediately removed from the furnace hot zone, allowing for rapid cooling in the  $\text{H}_2$  and Ar atmosphere. The sample was subsequently recovered from the quartz tube once sufficiently cool.

**Transfer.** A PMMA scaffold (8% wt. in anisole, 495k molecular weight) was spin-cast on to the graphene side of the sample at 4500 rpm for 60 s and then cured at  $180^\circ\text{C}$  for 90 s. The underlying copper were etched by floating the sample on an iron(III) chloride + hydrochloric acid solution for several hours, until just a transparent PMMA/graphene film remained suspended on the surface. This was thoroughly cleaned by transferring and floating onto fresh DI water several times. Following this, the sample was transferred to a 30% hydrochloric acid solution for 5 min, and then rinsed again in DI water for 30 min. Finally the graphene is transferred to a holey silicon nitride TEM grid, left to dry, and then heated to  $150^\circ\text{C}$  for 15 min to remove water. The PMMA is removed by heating in air at  $350^\circ\text{C}$  for several hours.

**Deposition of Fe Precursor.**  $\text{FeCl}_3$  (Alfar Aser 157740) was dissolved in acetone producing an  $\text{FeCl}_3$  solution with a

concentration of  $0.1\text{g}/10 \text{ mL}$ . This was drop-cast ( $30 \mu\text{l}$ ) directly onto the TEM grid with cleaned graphene on it. This resulted in a substantial increase in the number of heavy atoms on the surface of graphene compared to graphene without the addition of  $\text{FeCl}_3$ .

**Electron Microscopy.** AC-TEM was performed using the Oxford-JEOL JEM-2200MCO FEGTEM with CEOS hexapole image aberration corrector, operating at an accelerating voltage of 80 kV. TEM images with a color LUT are produced using ImageJ with “gem” or “fire” LUT. Defects were created using our previously reported method in ref 20. HRTEM images are typically taken with small defocus values around 1 nm.

**Density Functional Theory (DFT) Calculations.** Spin-polarized calculations were performed within the generalized gradient approximation of Perdew–Burke–Ernzerhof (PBE) functional<sup>34</sup> using Vienna ab initio simulation package (VASP) code.<sup>35</sup> Vanderbilt pseudopotentials<sup>36</sup> are also used in this calculation. The unit cells containing Fe atoms are constructed from pristine graphene of 240 carbon atoms. In constructing the super cell for simulation, we contain a vacuum region of  $30 \text{ \AA}$  in the z direction. The basis set contains plane waves up to an energy cutoff of 400 eV. The Brillouin zone was sampled using a  $(3 \times 3 \times 1)$   $\Gamma$ -centered mesh. When structural relaxations are performed, the structure is fully relaxed until the force on each atom is smaller than  $0.02 \text{ eV}/\text{\AA}$ .

## ■ ASSOCIATED CONTENT

### S Supporting Information

Quantitative analysis on the difference between two types of Fe dimer in graphene vacancy. Difference of total energy before and after the ejection of one Fe atom. Atomic model used for DFT calculation to investigate the relationship between separation distance and magnetic moment. Relative formation energy and magnetic moment of Fe dimer in two monovacancies with different separation distance. This material is available free of charge via the Internet at <http://pubs.acs.org>.

## ■ AUTHOR INFORMATION

### Corresponding Authors

\*E-mail: gdlee@snu.ac.kr.

\*E-mail: jamie.warner@materials.ox.ac.uk.

### Notes

The authors declare no competing financial interest.

## ■ ACKNOWLEDGMENTS

J.H.W. thanks the support from the Royal Society and Balliol College, Oxford. Z.H. has been supported by China Scholarship Council and China Oxford Scholarship Fund. G.-D.L and E.Y acknowledge support from the National Institute of Supercomputing and Networking/Korea Institute of Science and Technology Information with supercomputing resources (KSC-2013-C3-005) and support from the National Research Foundation of Korea under Basic Science Research (No. 2010-0012670).

## ■ REFERENCES

- (1) Castro Neto, A. H.; Guinea, F.; Peres, N. M. R.; Novoselov, K. S.; Geim, A. K. The Electronic Properties of Graphene. *Rev. Mod. Phys.* **2009**, *81*, 109–162.
- (2) Zhou, S. Y.; Siegel, D. A.; Fedorov, A. V.; Lanzara, A. Metal to Insulator Transition in Epitaxial Graphene Induced by Molecular Doping. *Phys. Rev. Lett.* **2008**, *101*, 086402.

- (3) Elias, D. C.; Nair, R. R.; Mohiuddin, T. M. G.; Morozov, S. V.; Blake, P.; Halsall, M. P.; Ferrari, A. C.; Boukhvalov, D. W.; Katsnelson, M. I.; Geim, A. K.; et al. Control of Graphene's Properties by Reversible Hydrogenation: Evidence for Graphane. *Science* **2009**, *323*, 610–613.
- (4) Bae, S.; Kim, H.; Lee, Y.; Xu, X.; Park, J.-S.; Zheng, Y.; Balakrishnan, J.; Lei, T.; Kim, H. R.; Song, Y. Il; et al. Roll-to-Roll Production of 30-Inch Graphene Films for Transparent Electrodes. *Nat. Nanotechnol.* **2010**, *5*, 574–578.
- (5) Blake, P.; Brimicombe, P. D.; Nair, R. R.; Booth, T. J.; Jiang, D.; Schedin, F.; Ponomarenko, L. A.; Morozov, S. V.; Gleeson, H. F.; Hill, E. W.; et al. Graphene-Based Liquid Crystal Device. *Nano Lett.* **2008**, *8*, 1704–1708.
- (6) Schedin, F.; Geim, A. K.; Morozov, S. V.; Hill, E. W.; Blake, P.; Katsnelson, M. I.; Novoselov, K. S. Detection of Individual Gas Molecules Adsorbed on Graphene. *Nat. Mater.* **2007**, *6*, 652–655.
- (7) Wang, Y.; Huang, Y.; Song, Y.; Zhang, X.; Ma, Y.; Liang, J.; Chen, Y. Room-Temperature Ferromagnetism of Graphene. *Nano Lett.* **2009**, *9*, 220–224.
- (8) Mao, Y.; Yuan, J.; Zhong, J. Density Functional Calculation of Transition Metal Adatom Adsorption on Graphene. *J. Phys. Condens. Matter* **2008**, *20*, 115209.
- (9) Cao, C.; Wu, M.; Jiang, J.; Cheng, H.-P. Transition Metal Adatom and Dimer Adsorbed on Graphene: Induced Magnetization and Electronic Structures. *Phys. Rev. B* **2010**, *81*, 205424.
- (10) Sevinçli, H.; Topsakal, M.; Durgun, E.; Ciraci, S. Electronic and Magnetic Properties of 3d Transition-Metal Atom Adsorbed Graphene and Graphene Nanoribbons. *Phys. Rev. B* **2008**, *77*, 195434.
- (11) Chan, K. T.; Neaton, J. B.; Cohen, M. L. First-Principles Study of Metal Adatom Adsorption on Graphene. *Phys. Rev. B* **2008**, *77*, 235430.
- (12) Wei, D.; Liu, Y.; Wang, Y.; Zhang, H.; Huang, L.; Yu, G. Synthesis of N-Doped Graphene by Chemical Vapor Deposition and Its Electrical Properties. *Nano Lett.* **2009**, *9*, 1752–1758.
- (13) Ci, L.; Song, L.; Jin, C.; Jariwala, D.; Wu, D.; Li, Y.; Srivastava, A.; Wang, Z. F.; Storr, K.; Balicas, L.; et al. Atomic Layers of Hybridized Boron Nitride and Graphene Domains. *Nat. Mater.* **2010**, *9*, 430–435.
- (14) Zhan, D.; Sun, L.; Ni, Z. H.; Liu, L.; Fan, X. F.; Wang, Y.; Yu, T.; Lam, Y. M.; Huang, W.; Shen, Z. X. FeCl<sub>3</sub>-Based Few-Layer Graphene Intercalation Compounds: Single Linear Dispersion Electronic Band Structure and Strong Charge Transfer Doping. *Adv. Funct. Mater.* **2010**, *20*, 3504–3509.
- (15) Kim, N.; Kim, K. S.; Jung, N.; Brus, L.; Kim, P. Synthesis and Electrical Characterization of Magnetic Bilayer Graphene Intercalate. *Nano Lett.* **2011**, *11*, 860–865.
- (16) Farmer, D. B.; Golizadeh-Mojarad, R.; Perebeinos, V.; Lin, Y.-M.; Tulevski, G. S.; Tsang, J. C.; Avouris, P. Chemical Doping and Electron-Hole Conduction Asymmetry in Graphene Devices. *Nano Lett.* **2009**, *9*, 388–392.
- (17) Shi, Y.; Kim, K. K.; Reina, A.; Hofmann, M.; Li, L.-J.; Kong, J. Work Function Engineering of Graphene Electrode via Chemical Doping. *ACS Nano* **2010**, *4*, 2689–2694.
- (18) Bangert, U.; Pierce, W.; Kepaptsoglou, D. M.; Ramasse, Q.; Zan, R.; Gass, M. H.; Berg, J. A.; Van den Boothroyd, C. B.; Amani, J.; Hofäss, H. Ion Implantation of Graphene-Toward IC Compatible Technologies. *Nano Lett.* **2013**, *13*, 4902–4907.
- (19) Robertson, A. W.; Montanari, B.; He, K.; Kim, J.; Allen, C. S.; Wu, Y. A.; Olivier, J.; Neethling, J.; Harrison, N.; Kirkland, A. I.; et al. Dynamics of Single Fe Atoms in Graphene Vacancies. *Nano Lett.* **2013**, *13*, 1468–1475.
- (20) Robertson, A. W.; Allen, C. S.; Wu, Y. A.; He, K.; Olivier, J.; Neethling, J.; Kirkland, A. I.; Warner, J. H. Spatial Control of Defect Creation in Graphene at the Nanoscale. *Nat. Commun.* **2012**, *3*, 1144.
- (21) Krasheninnikov, A. V.; Lehtinen, P. O.; Foster, A. S.; Pyykkö, P.; Nieminen, R. M. Embedding Transition-Metal Atoms in Graphene: Structure, Bonding, and Magnetism. *Phys. Rev. Lett.* **2009**, *102*, 126807.
- (22) Cretu, O.; Krasheninnikov, A. V.; Rodríguez-Manzo, J. A.; Sun, L.; Nieminen, R. M.; Banhart, F. Migration and Localization of Metal Atoms on Strained Graphene. *Phys. Rev. Lett.* **2010**, *105*, 196102.
- (23) Chisholm, M. F.; Duscher, G.; Windl, W. Oxidation Resistance of Reactive Atoms in Graphene. *Nano Lett.* **2012**, *12*, 4651–4655.
- (24) Wang, W. L.; Santos, E. J. G.; Jiang, B.; Cubuk, E. D.; Ophus, C.; Centeno, A.; Pesquera, A.; Zurutuza, A.; Ciston, J.; Westervelt, R.; et al. Direct Observation of a Long-Lived Single-Atom Catalyst Chiseling Atomic Structures in Graphene. *Nano Lett.* **2014**, *14* (2), 450–455.
- (25) Lee, J.; Zhou, W.; Pennycook, S. J.; Idrobo, J.-C.; Pantelides, S. T. Direct Visualization of Reversible Dynamics in a Si<sub>6</sub> Cluster Embedded in a Graphene Pore. *Nat. Commun.* **2013**, *4*, 1650.
- (26) Warner, J. H.; Margine, E. R.; Mukai, M.; Robertson, A. W.; Giustino, F.; Kirkland, A. I. Dislocation-Driven Deformations in Graphene. *Science* **2012**, *337*, 209–212.
- (27) Goodman, P.; Moodie, A. F. Numerical Evaluations of N-Beam Wave Functions in Electron Scattering by the Multi-Slice Method. *Acta Crystallogr.* **1974**, *A30*, 280–290.
- (28) Cowley, J. M.; Moodie, A. F. The Scattering of Electrons by Atoms and Crystals. I. A New Theoretical Approach. *Acta Crystallogr.* **1957**, *10*, 609–619.
- (29) Yazayev, O. V.; Helm, L. Defect-Induced Magnetism in Graphene. *Phys. Rev. B* **2007**, *75*, 125408.
- (30) Topsakal, M.; Aktürk, E.; Sevinçli, H.; Ciraci, S. First-Principles Approach to Monitoring the Band Gap and Magnetic State of a Graphene Nanoribbon via Its Vacancies. *Phys. Rev. B* **2008**, *78*, 235435.
- (31) Zhang, Y.; Talapatra, S.; Kar, S.; Vajtai, R.; Nayak, S. K.; Ajayan, P. M. First-Principles Study of Defect-Induced Magnetism in Carbon. *Phys. Rev. Lett.* **2007**, *99*, 107201.
- (32) Dai, X. Q.; Zhao, J. H.; Xie, M. H.; Tang, Y. N.; Li, Y. H.; Zhao, B. First-Principle Study of Magnetism Induced by Vacancies in Graphene. *Eur. Phys. J. B* **2011**, *80*, 343–349.
- (33) Pesin, D.; MacDonald, A. H. Spintronics and Pseudospintrronics in Graphene and Topological Insulators. *Nat. Mater.* **2012**, *11*, 409–416.
- (34) Perdew, J. P.; Burke, K.; Ernzerhof, M. Generalized Gradient Approximation Made Simple. *Phys. Rev. Lett.* **1996**, *77*, 3865–3868.
- (35) Kresse, G.; Furthmüller, J. Efficient Iterative Schemes for Ab Initio Total-Energy Calculations Using a Plane-Wave Basis Set. *Phys. Rev. B* **1996**, *54*, 11169–11186.
- (36) Vanderbilt, D. Soft Self-Consistent Pseudopotentials in a Generalized Eigenvalue Formalism. *Phys. Rev. B* **1990**, *41*, 7892–7895.